British Acoustical Society
Nonlinear Underwater Acoustics Meeting
University of Birmingham, Birmingham, England
1-2 April 1971

APPROXIMATE SCALING LAWS FOR PARAMETRIC SONAR TRANSMITTER DESIGN

by
Robert H. Mellen, William L. Konrad, David G. Browning

New London Laboratory, Naval Underwater Systems Center
New London, Connecticut 06320, USA

ABSTRACT

The complexities of nonlinear radiation theory tend to make the design of parametric transmitters a cut-and-try procedure. Thus far we have only Westervelt's end-fire radiator solution to serve as a guide. However, his model assumes weak interactions that are limited to the near field by primary wave absorption. For Sonar design, we propose a strong interaction modification where primary wave saturation governs the near field limit. Approximate scaling laws for source level and directivity are presented along with supporting experimental measurements.

* * *

In spite of the complexities of nonlinear wave theory it might be expected that satisfactory approximate solutions to parametric Sonar radiation problems could be achieved. However, with perturbation methods, the results are often less than adequate. The reason is that we are interested in the highest attainable source levels and then higher order perturbations become as important as the first. It is therefore not surprising that plane and spherical wave models are so attractive since the saturated field problem becomes tractable if not too realistic.

Figure 1 shows the usual "one dimensional" model of a circular piston radiator where the field is collimated to a distance R_o and diverges spherically thereafter. The three waveforms illustrate oscilloscope pressure vs. time traces measured at the corresponding points in the field. The waveform, which is initially sinusoidal at A , becomes sawtooth at B due to the finite amplitude overtaking effect, and then diminishes in amplitude (C) as the wave diverges (phase effects are neglected).

A measure of the nonlinearity of the radiation field is given by the saturation index x :

$$X = \omega_o T = \epsilon P_o R_o \omega_o / \rho_o c_o^3$$

which defines the overtaking time T of a sine wave of peak pressure P_o and angular frequency ω_o, measured at collimation distance R_o (see Appendix 1). Expressed in terms of R.M.S. source level L_S we have:

$$L_S = 20 \log (P_o R_o) - 3 = 180 - 20 \log f_o(\text{kHz}) + 20 \log x \text{ dB//1 } \mu\text{bm}$$

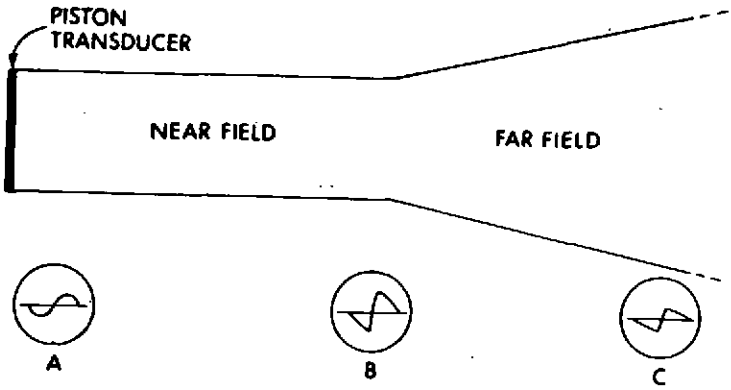

PISTON TRANSDUCER FIELD AND WAVE FORMS

Fig. 1

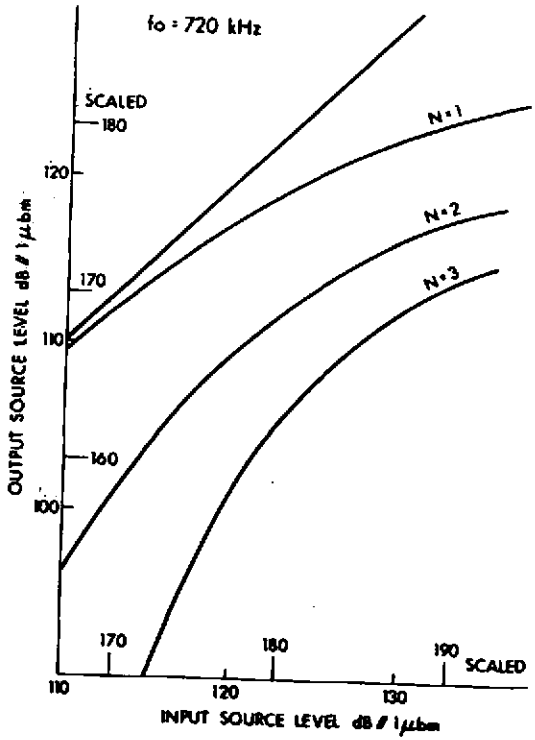

* Field Saturation Curve

If, for a particular set of experimental conditions (in this case a 10 cm diameter piston at 720 kHz), the actual source level measured at a large distance from the source is plotted against the equivalent input source level, a curve similar to Fig. 2 is obtained. By adding 20 log f_o to the scales we obtain a "generalized" input-output curve referred to 1 kHz. As the scaled input exceeds 180 dB ($x = 1$) it is seen that the harmonics $N = 2,3$ grow at the expense of the fundamental ($N = 1$) which then tends to deviate from linear as the wave becomes saturated.

For parametric end-fire radiation (Ref. 1-7) two high frequencies are fed to the piston radiator as shown in Fig. 3. The difference frequency field is plotted as a function of range as shown in Fig. 4. (The mean primary frequency in this example is also 720 kHz.) Figure 5 shows the difference frequency beam patterns. Note that in the far field, the difference frequency pressure tends to decrease as the square of the frequency downshift ratio while the directivity goes as the first power. This behavior is predicted by Westervelt (Ref. (1)) formula (see Appendix 2). However, in our case (Ref. (2)) the radiator length is determined by primary wave saturation rather than by absorption.

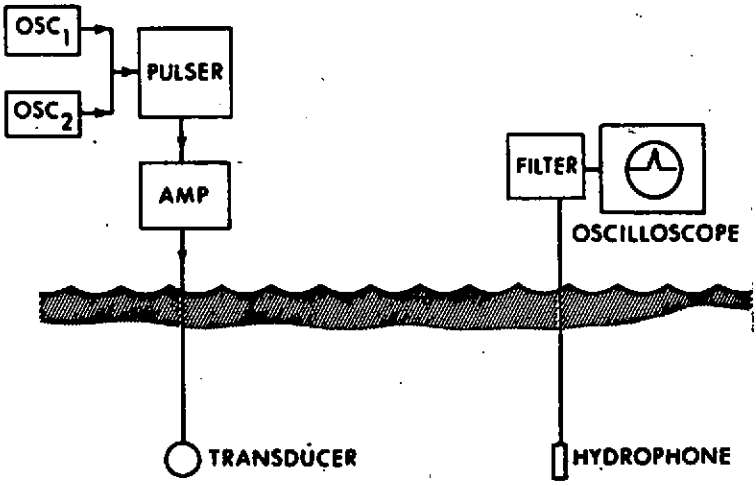

PARAMETRIC ARRAY EXPERIMENT

Fig. 3

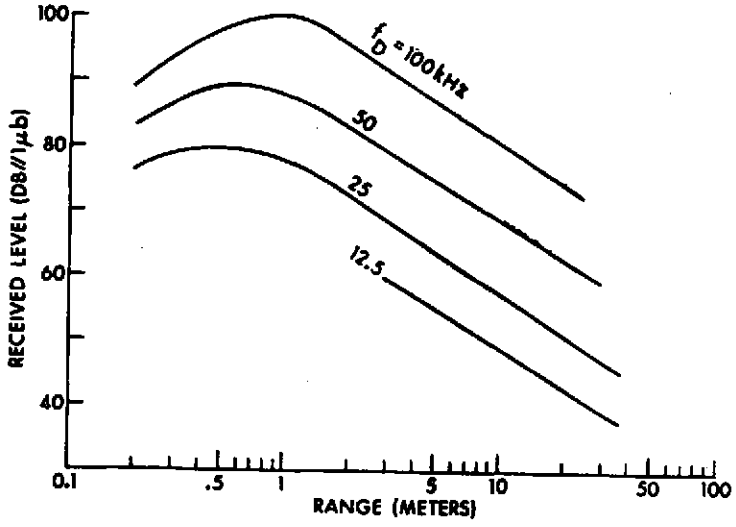

Fig. 4 - Difference Frequency Levels vs. Range for Various Frequencies

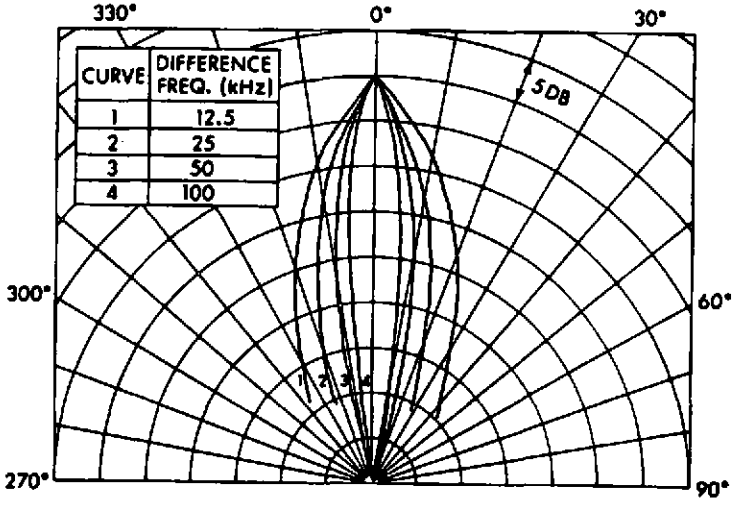

Fig. 5 - Difference Frequency Beam Patterns

Figure 6 shows the 50 kHz field plots for various primary levels. The associated directivity patterns are shown in Fig. 7. Note that in the far field the difference frequency level begins to fall linearly with the input and then tends to square law below saturation. The directivity however tends to increase, apparently approaching the primary directivity as an upper limit. The 50 kHz results are summarized in Fig. 8 which shows the input-output source level curve and the directivity index curve. (Input source level here is based on the sum of the powers of the two primary components.) The results can be "generalized" to 1 kHz by adding 40 log f_o/f to the secondary scale and 20 log f_o to both scales as shown in Fig. 9. The directivity is scaled by adding 10 log f_o/f to the secondary index and then subtracting the result from the primary directivity index (see Appendix 2).

The empirical scaling curves of Fig. 9 have proved to give reasonably good predictions for a variety of conditions. Tables 1-3 give a summary of results obtained in recent experiments for the three different piston transducers described. The pertinent experimental conditions are listed together with a compilation of the source levels and directivity indices for various input levels. The data are repeated with the scaling corrections applied and are also plotted in Fig. 10. Considering the apparent magnitude of the experimental error, the data show reasonably good consistency and agreement with the earlier results except for generally higher values of directivity index.

Summarizing the problem of parametric transmitter design: below saturation there is a tradeoff between secondary source level and directivity where the secondary source level varies as the square of the primary and the directivity begins to decrease as saturation is approached; above saturation the secondary source level tends to increase linearly with the primary, while the directivity decreases as the -1/2 power. As saturation further increases, secondary wave distortion must eventually become an important consideration when harmonics of the difference frequency grow to appreciable magnitude.

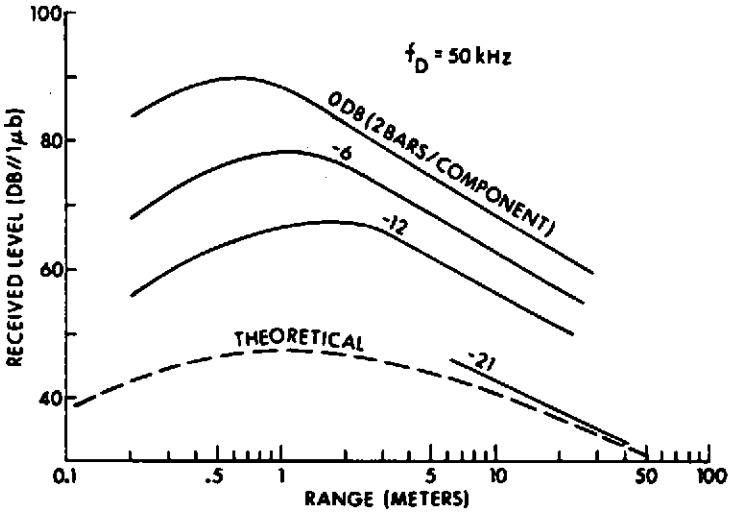

Fig. 6 - 50 kHz Level vs. Range for Various Primary Levels

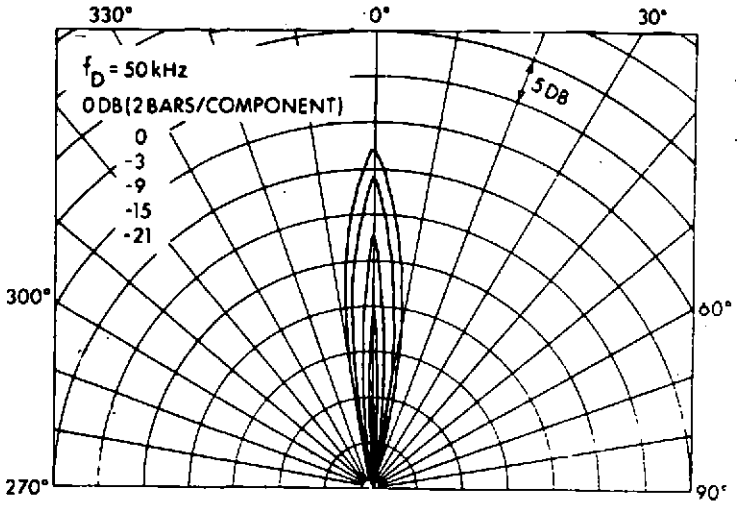

Fig. 7 - 50 kHz Beam Patterns for Various Levels

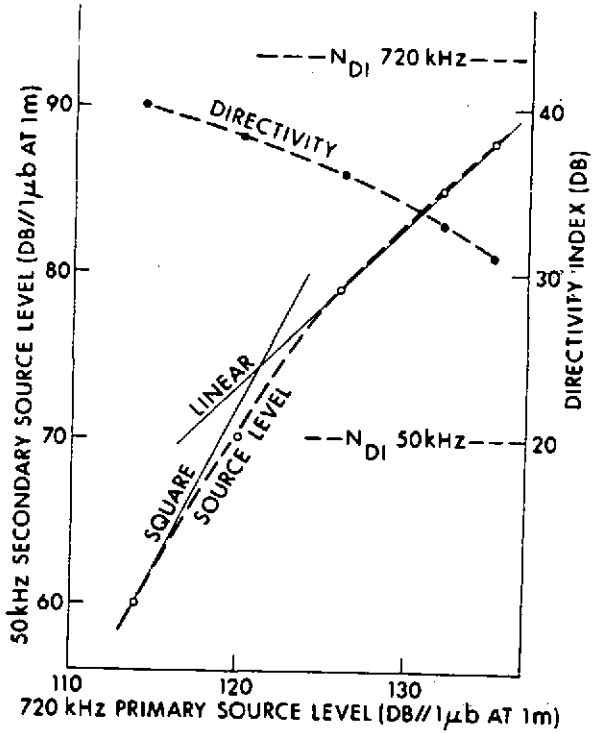

Fig. 8 - Source Level and Directivity Curves 720 kHz

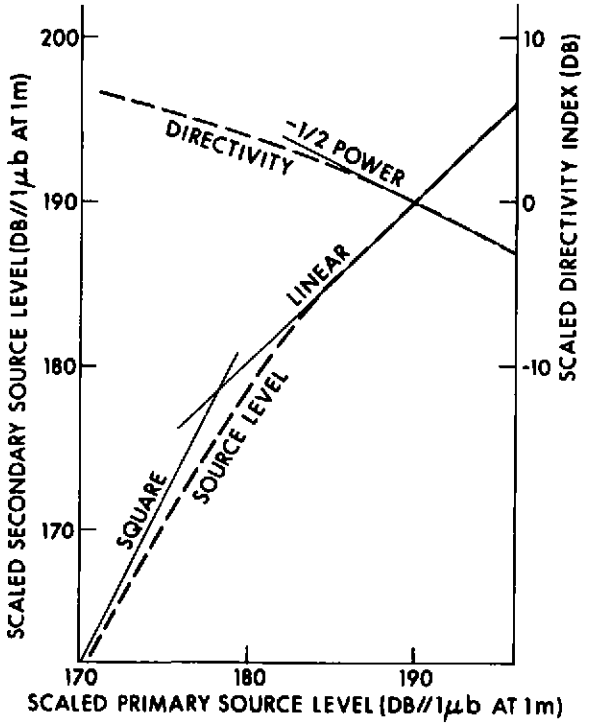
200
190
180
170
10
0
-10
SCALED SECONDARY SOURCE LEVEL (DB//1μb AT 1m)
SCALED DIRECTIVITY INDEX (DB)
DIRECTIVITY
-1/2 POWER
LINEAR
SQUARE
SOURCE LEVEL
170
180
190
SCALED PRIMARY SOURCE LEVEL (DB//1μb AT 1m)

Fig. 9

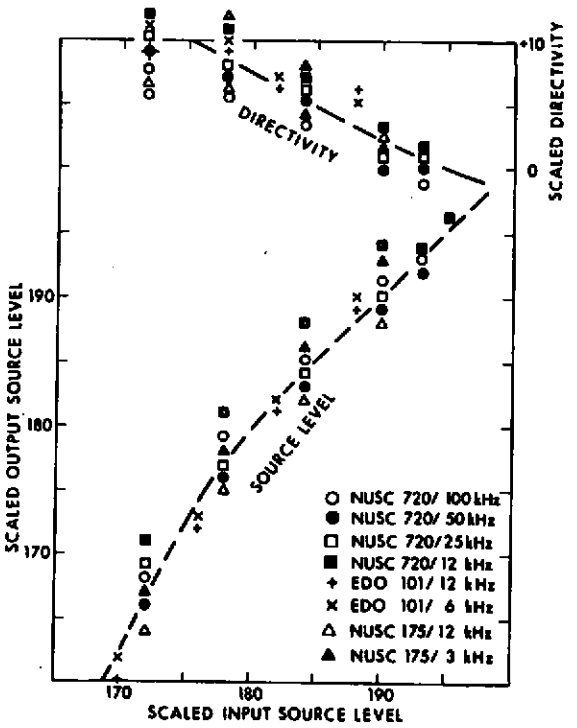
+10
0
SCALED DIRECTIVITY
DIRECTIVITY
190
180
170
SCALED OUTPUT SOURCE LEVEL
SOURCE LEVEL
NUSC 720/ 100 kHz
NUSC 720/ 50 kHz
NUSC 720/ 25 kHz
NUSC 720/ 12 kHz
EDO 101/ 12 kHz
EDO 101/ 6 kHz
NUSC 175/ 12 kHz
NUSC 175/ 3 kHz
170
180
190
SCALED INPUT SOURCE LEVEL

Fig. 10

TABLE 1

NUSC/720

PISTON 10 cm. dia.

fo = 720 kHz

N_{DI} = 43 dB

L_{SO} = 136 dB // 1 μbm

R_O = 4 M R = 11M

	100 kHz		50 kHz		25 kHz		12.5 kHz	
INPUT dB	L_S	N_{DI}	L_S	N_{DI}	L_S	N_{DI}	L_S	N_{DI}
0	101	33	88	31	77	28	68	26
- 3	99	35	85	32	74	29	66	28
- 9	93	38	79	36	68	35	60	32
-15	87	40	72	38	60	36	53	36
-21	76	40	62	40	53	38	43	38
193	193	-1	192	0	193	0	196	1
190	191	1	189	1	190	1	189	3
184	185	4	183	5	189	7	188	7
178	179	6	176	7	176	8	181	11
172	168	6	166	9	169	10	171	13

TABLE 2

EDO/101

PISTON 25 cm. dia.

f_o = 250 kHz

N_{DI} = 42 dB

L_{SO} = 140 dB// 1 µbm

R_O = 8 M R = 42 M

	12 kHz		6 kHz	
INPUT dB	L_S	N_{DI}	L_S	N_{DI}
0 dB	89	35	78	32
- 6	81	36	70	35
-12	72	38	60	35
-18	60	39	50	37
188	189	6	190	6
182	181	7	182	9
176	172	9	172	9
170	160	10	162	11

TABLE 3

NUSC/175

PISTON 40 x 40 cm.

f_o = 175 kHz

N_{DI} = 45 dB

L_{SO} = 145 dB // 1 µbm

R_O = 16 M R = 42 M

	12 kHz		3 kHz	
INPUT dB	L_S	N_{DI}	L_S	N_{DI}
0	98	34	78	28
- 6	92	38	71	34
-12	84	39	63	38
-18	73	41	52	-
190	189	1	193	1
184	183	5	186	7
178	175	6	178	11
172	164	8	167	-

REFERENCES

(1) P. J. Westervelt, "Parametric Acoustic Array," J. Acoust. Soc. Am. 35, 535-537 (1963).

(2) J. L. S. Bellin and R. T. Beyer, "Experimental Investigation of an End-Fire Array," J. Acoust. Soc. Am. 34, 1051-1054 (1962).

(3) H. O. Berktay, "Some Proposals for Underwater Transmitting Applications of Nonlinear Acoustics," J. Sound Vib. (1967) 6, (2) 244-254.

(4) T. G. Muir and J. E. Blue, "Experiments on the Acoustic Modulation of Large Amplitude Waves," J. Acoust. Soc. Am. 46, 227-232 (1969).

(5) R. H. Mellen, D. G. Browning and W. L. Konrad, "Parametric Sonar Transmitting Array Measurements," J. Acoust. Soc. Am. 49, 90(A) (1971).

(6) V. A. Zverev and A. I. Kalachev, Sov. Phys. Acoust. 14 (2), 173-178 (1968).

(7) H. Hobaek, "Experimental Investigation of an End-Fire Array," J. Sound Vib. (1967) 6 (3), 460-463.

APPENDIX 1

For plane waves, the nonlinear wave equation is taken as:

$$\frac{\partial P}{\partial r} = \frac{\epsilon}{2\rho_o c_o^3} \frac{\partial P^2}{\partial \tau} \qquad (1)$$

P is the instantaneous pressure

$\epsilon = 4$ is the nonlinearity parameter for water

r is the distance

$\tau = t - r/c_o$ where t is time

ρ_o is the normal density

c_o is the normal sound speed.

The solution of Eq. (1) is:

$$\tau_{P,r} = \tau_{P,o} - \epsilon P r / \rho_o c_o^3$$

Let $P = P_o \cos \omega_o t$ at $r = 0$ and let $x = \omega_o T$,

($r = R_o$ $\tau = \tau_{P_o}$) where R_o is the collimation distance of the wave.

Then

$$x = \epsilon P_o R_o \omega_o / \rho_o c_o^3$$

In terms of RMS source level L_S :

$$L_S = 20 \log (P_o R_o) - 3 = 180 - 20 \log f_{kHz} + 20 \log x$$

dB// 1 μbar

where P_o is in μbars and R_o is in meters.

The frequency f is in kiloherts.

APPENDIX 2

Westervelt's[1] equation can be written:

$$P = \frac{\epsilon P_o^2 k^2 S L}{4\pi \rho_o c_o^2 r \left[1 + \left(\frac{2kL \sin^2\frac{\theta}{2}}{2}\right)^2\right]^{1/2}}$$

where P is the difference frequency peak pressure at r, θ

P_o is the peak pressure of each primary component

S is the piston area = πa^2 (a = radius)

k is the difference frequency wave number

L = 1/2 α is the absorption length

r is the distance ($r \gg L$)

θ is the half beam angle

If we let the saturation index be:

$$\chi = \epsilon P_o k_o R_o / \rho_o c_o^2 = R_o/L$$

where k_o is the mean primary frequency wave number and R_o is the primary wave collimation distance. Substituting $R_o = k_o S/2\pi$ we have:

$$rP = \frac{\frac{1}{2} P_o R_o (k/k_o)^2}{\left[1 + \left(\frac{2k R_o}{\chi} \sin^2\frac{\theta}{2}\right)^2\right]^{1/2}}$$

Taking for the primary source level:

$$L_{sp} = 20 \log P_o R_o$$

where P_o is the peak pressure μb per component and R_o is the collimation distance in meters, then we have finally for the RMS secondary source level L_{SS} :

$$L_{SS} = 20 \log(Pr) - 3 = L_{sp} - 40 \log(f_o/f) - 9$$

dB // 1 μbm

representing the saturated condition ($\chi > 1$).

The secondary directivity index is given by:

$$N_{DIS} \doteq 20 \log(\pi/2\theta_o) = 16 \log(\pi^3 k R_o/16\chi)$$

where $2\theta_o$ is the -3 dB beamwidth. The primary directivity is given by:

$$N_{DIP} \doteq 10 \log(2k_o R_o)$$

Therefore:

$$N_{DIS} \doteq N_{DIP} - 10\log(f_0/f) - 10\log x$$

In the "plane wave" approximation we again assume two primary frequencies and compute second order terms for the difference frequency from the plane wave solution of Appendix 1. To account for radiation leakage of the secondary wave we also introduce a secondary wave collimation distance:

$$R = R_0 (K/K_0)$$

Then we find for P axial:

$$P \doteq \frac{\epsilon P_0^2}{2\rho_0 c_0^2} Kr \qquad 0 < r < R$$

$$P \doteq \frac{\epsilon P_0^2}{2\rho_0 c_0^2} KR \ln\left(1 + \frac{r}{R}\right) \qquad 0 < r < L < R_0$$

$$rP \to \frac{1}{2} R_0 P_0 \left(K/K_0\right)^2 \qquad r >> L$$

Where L is the primary wave discontinuity distance.

When the directivity function is included:

$$rP = \frac{\frac{1}{2} R_0 P_0 \left(K/K_0\right)^2}{\left[1 + \left(\frac{\delta K R_0}{\pi} \sin^2\frac{\theta}{2}\right)^2\right]^{1/2} \left[1 + (K_0 \sin\theta)^2\right]^{1/2}} \qquad x > 1$$